

# Afterslip and aftershocks in the rate-and-state friction law

Agnès Helmstetter<sup>1</sup> and Bruce E. Shaw<sup>2</sup>

<sup>1</sup> Laboratoire de Géophysique Interne et Tectonophysique, Université Joseph Fourier and Centre National de la Recherche Scientifique, Grenoble, France

<sup>2</sup> Lamont-Doherty Earth Observatory, Columbia University, New York

## Abstract.

We study how a stress perturbation generated by a mainshock affects a population of faults obeying a rate-state friction law. Depending on the model parameters and on the initial state, the fault exhibits aftershocks, slow earthquakes, or decaying afterslip. We found several regimes with slip rate decaying as a power-law of time, with different characteristic times and exponents. The complexity of the model makes it unrealistic to invert for the friction law parameters from afterslip data. We modeled afterslip measurements for the Southern California Superstition Hills earthquake using the complete rate-and-state law, and found a huge variety of model parameters that can fit the observed data. In particular, it is impossible to distinguish the stable velocity strengthening regime ( $A > B$ ) from the (potentially) unstable velocity weakening regime ( $B > A$  and stiffness  $k < k_c$ ). Therefore, it is not necessary to involve small scale spatial or temporal fluctuations of friction parameters  $A$  or  $B$  in order to explain the transition between stable sliding and seismic slip. In addition to  $B/A$  and stiffness  $k/k_c$ , the fault behavior is strongly controlled by stress levels following an event. Stress heterogeneity can thus explain most of the variety of postseismic behavior observed in nature. Afterslip will induce a progressive reloading of faults that are not slipping, which can trigger aftershocks. Using the relation between stress and seismicity derived from the rate-and-state friction law, we estimate the aftershock rate triggered by afterslip. Aftershock rate does not simply scale with stress rate, but exhibits different characteristic times and sometimes a different power-law exponent. Afterslip is thus a possible candidate to explain observations of aftershock rate decaying as a power-law of time with an Omori exponent that can be either smaller or larger than 1.

## 1. Introduction

Most shallow large earthquakes are followed by a significant postseismic deformation, and by an increase in seismic activity, which both start immediately after the mainshock and last for several years. The link between aseismic afterslip and aftershock activity is however not clear. The cumulative moment released by aftershocks is usually much lower than the one associated with afterslip, which implies that postseismic deformation is unlikely to be due to aftershock activity. The similar time decay and duration of postseismic deformation and aftershocks rather suggests that aftershocks are induced by afterslip [Wennerberg and Sharp, 1997; Schaff *et al.*, 1998; Perfettini and Avouac, 2004; Hsu *et al.*, 2006]. But there are alternative models which explain aftershock triggering by the static [Dieterich, 1994] or dynamic [Gomberg *et al.*, 1998] stress change associated with the mainshock, or by fluid flow [Nur and Booker, 1972].

Postseismic deformation is most often localized around the rupture zone, and is thus modeled as afterslip on the mainshock fault. However, there are observations of long-range diffuse deformation following large earthquakes [Nur and Mavko, 1972], which can be modeled by visco-elastical relaxation of the lower crust or upper mantle. Another potential candidate for postseismic deformation is poro-elastic deformation. Distinguishing between the different mechanisms is difficult based on available data [Montési, 2004]. In some cases, several processes have to be involved to fit

the data [Pollitz *et al.*, 2006; Freed *et al.*, 2006]. Afterslip is often comparable with postseismic slip (see [Pritchard and Simons, 2006] for a review on afterslip in subduction zones), even if there are very large variations in the amount of afterslip from one event to another one [Melbourne *et al.*, 2002; Marone, 1998; Pritchard and Simons, 2006]. For instance, the  $m_w$ 7.6 1994 Sanriku-Haruka-Oki earthquake in Japan had very large afterslip, with cumulative seismic moment a little larger than the coseismic moment [Heki *et al.*, 1997]. Takai *et al.* [1999] also reported afterslip as large, in term of seismic moment, as coseismic slip for a much smaller  $m_w = 5.7$  earthquake in the same area. This suggest that afterslip scales with coseismic slip.

The rate-and-state friction law, introduced by Dieterich [1979] based on laboratory friction experiments, has been frequently used to model both aseismic deformation [e.g., Marone *et al.*, 1991], slow earthquakes [e.g., Yoshida and Kato, 2003], and seismic activity [e.g., Dieterich, 1994]. Depending on the parameters of the rate-and-state friction law, the model is either stable (aseismic slip), or produce slip instabilities (earthquakes). In the unstable regime, the rate-and-state friction law provides a relation between stress history and seismicity [Dieterich, 1994]. This relation can be used to predict the seismicity rate triggered by any stress change, such as static [Dieterich, 1994] or dynamic [Gomberg *et al.*, 1998] stress change induced by a mainshock, postseismic slip, or transient deformation associated with intrusions or eruptions [Dieterich *et al.*, 2000], slow earthquakes [Segall *et al.*, 2006] or tides [Cochran *et al.*, 2004]. Extensions of the original theory to include stress heterogeneity as a fundamental aspect of aftershock process has further improved matches with observations, including where aftershocks occur and modifications to the time dependence of the decay

[Marsan, 2006; Helmstetter and Shaw, 2006]. This extension explains why many aftershocks occur on the mainshock rupture area, where stress decreases on average after the mainshock.

Previous studies have modeled afterslip using the rate-and-state friction law [Scholz, 1990; Marone et al., 1991; Marone, 1998; Wennerberg and Sharp, 1997; Schaff et al., 1998; Miyazaki et al., 2004; Montési, 2004], or a simpler rate-dependent friction law [Perfettini and Avouac, 2004; Hsu et al., 2006]. These studies have assumed that afterslip is associated with stable faults in the velocity strengthening regime. They have also assumed that faults are close to the steady state regime during afterslip, which amounts to neglect of fault healing. With this approximation, the friction coefficient only depends on slip velocity, which simplifies the analysis. These studies have been very successful in matching afterslip data [Scholz, 1990; Marone et al., 1991; Marone, 1998; Wennerberg and Sharp, 1997; Miyazaki et al., 2004; Montési, 2004]. However, they also bring new problems. The observation that afterslip and earthquakes often occur on the same parts of a fault requires either small-scale spatial [Miyazaki et al., 2004] or temporal [Wennerberg and Sharp, 1997] variations in the friction parameters.

In this work, we study analytically and numerically the postseismic slip in the rate-and-state model, without using the steady state approximation. We show that afterslip is not limited to stable faults, but can also occur in seismogenic zones. We also fit the model to the afterslip data measured following the 1987 Superstition Hills earthquake and analysed by Wennerberg and Sharp [1997].

Afterslip transfers stress from sliding to locked part of the fault, and is thus a potential mechanism for aftershock triggering [Wennerberg and Sharp, 1997; Schaff et al., 1998; Perfettini and Avouac, 2004; Hsu et al., 2006]. Dieterich [1994] noted that non-constant stressing following an earthquake can alter the aftershock decay rate, and give rise to Omori exponents larger than 1. The suggestion that afterslip triggers aftershocks is based on the observation that both afterslip and aftershock rate roughly decay as the inverse of the time since the mainshock. However, there is a priori no reason to expect that aftershock rate is proportional to stress rate. In particular, in the rate-and-state friction model, earthquakes can be triggered at very long times following a stress change. The relation between stress history and seismicity rate is indeed complex and non-linear [Dieterich, 1994]. We thus use the complete rate-and-state friction law in order to model afterslip and aftershock activity. This allow us to better explain the temporal and spatial distribution of afterslip and aftershocks.

## 2. Rate-and-state friction law and afterslip

### 2.1. Slider-block model with rate-and-state friction

We use the rate and state friction formulation of Ruina [1983], based on [Dieterich, 1979]

$$\mu = \mu^* + A \ln \frac{V}{V^*} + B \ln \frac{\theta V^*}{D_c}. \quad (1)$$

where  $\mu^*$  and  $V^*$  are constants,  $A$  and  $B$  are friction parameters,  $D_c$  is the critical slip distance, and  $\theta$  is the state variable, which will evolve with slip and time. The state variable is often interpreted as the average age of contacts on the fault.

There are a couple of evolution laws for the state variable. Dieterich [1994] used the slowness law

$$\frac{d\theta}{dt} = 1 - \frac{V\theta}{D_c}, \quad (2)$$

Following Dieterich [1994], we model a fault by a slider-spring system. The friction coefficient of the block is given

by

$$\mu = \frac{\tau}{\sigma} = \frac{\tau_r - k\delta}{\sigma} \quad (3)$$

where  $k$  is the spring stiffness,  $\sigma$  is the normal stress,  $\tau$  the shear stress on the interface,  $\tau_r$  is the remotely applied stress acting on the fault in the absence of slip, and  $-k\delta$  is the decrease in stress due to fault slip. Expression (3) neglects inertia, and is thus only valid for low slip speed in the interseismic period. The stiffness is a function of the crack length  $l$  and shear modulus  $G$  [Dieterich, 1994]

$$k \approx G/l. \quad (4)$$

### 2.2. Steady state approximation

In the steady state regime  $\dot{\theta} = 0$ , the friction law (1) becomes

$$\mu_{ss}(V) = \mu^* + (A - B) \ln \frac{V}{V^*}. \quad (5)$$

If  $A > B$ , the friction law is velocity-strengthening, and the system is stable. In this regime, the state variable relaxes toward its steady state value when the slip exceeds the critical slip  $D_c$ , and at constant sliding velocity. If  $A < B$ , the steady state (5) is unstable, except during inertia controlled instabilities [Rice and Tse, 1986], and unless the system is too stiff. Ruina [1983] showed that, in order to produce slip instabilities ("earthquakes"), we need both  $B > A$  and  $k < k_c$ , where  $k_c$  is defined by

$$k_c = \frac{\sigma(B - A)}{D_c}. \quad (6)$$

Note that  $k_c$  defined by (6) is negative for  $A > B$ .

In the steady state approximation, the state variable is constant, there is thus no healing. This approximation  $\dot{\theta} = 0$  in (2) also requires that the slip speed is approximately constant equal to  $D_c/\theta$ . Therefore, it does not seem relevant to model afterslip, when slip speed decreases between coseismic slip speed ( $\approx m/s$ ) at very short times, to values lower than the long-term rate ( $\approx mm/yr \approx 10^{-10}m/s$ ) at large times.

Previous studies [Scholz, 1990; Marone et al., 1991; Wennerberg and Sharp, 1997; Marone, 1998; Schaff et al., 1998; Montési, 2004; Hsu et al., 2006] have used the rate-and-state friction law to model afterslip, assuming the fault is close to the steady state regime. They suggested that afterslip is produced within velocity-strengthening ( $A > B$ ) parts of the fault, below or above the seismogenic zone (where  $B > A$  to produce earthquakes). In these zones, there is a slip deficit after an earthquake, and thus an increase in Coulomb stress, which is relaxed during afterslip.

With the steady state approximation  $\dot{\theta} \approx 0$ , and without loading stress rate ( $\dot{\tau}_r = 0$ ), afterslip increases logarithmically with time [Scholz, 1990; Marone et al., 1991]

$$\delta = \frac{(A - B)\sigma}{k} \ln \left( \frac{kV_0 t}{\sigma(A - B)} + 1 \right) = V_0 t^* \ln \left( \frac{t}{t^*} + 1 \right) \quad (7)$$

where  $V_0$  is the initial slip speed and

$$t^* = \frac{\sigma(A - B)}{kV_0} \quad (8)$$

is a characteristic time for afterslip. Slip speed given by

$$V = \frac{V_0}{1 + t/t^*} \quad (9)$$

decreases as the inverse of time for  $t > t^*$ .

We can test the limit of validity of equation (7) by injecting the solution for the slip speed (9) and the state variable  $\theta = D_c/V_0$  back into the evolution law (2)

$$\dot{\theta} = 1 - \frac{V}{V_0} = 1 - \frac{1}{1 + t/t^*} \quad (10)$$

This shows that the steady state approximation (7) works only for very short times, when velocity is close to its initial value, but gets very bad when  $t > t^*$ . Thus it cannot explain the power law decay of afterslip rate with time.

Nevertheless, application of expression (7) provides a very good fit to afterslip data, with however significant discrepancies [Wennerberg and Sharp, 1997; Montési, 2004]. To better explain the data, Wennerberg and Sharp [1997] have used a more complex form of equation (1). They have also suggested to introduce a second state variable in (1), in order to explain apparent negative values of  $A$  obtained when inverting afterslip data, and to explain the transition between aseismic and seismic slip during the earthquake cycle.

Montési [2004] introduced a non-zero loading stress in order to better fit GPS data. But nobody has yet checked the consistency of the steady-state assumption and verified that  $\theta$  in the evolution law (2) is indeed negligible during afterslip. Only Marone *et al.* [1991] performed numerical simulations without the quasi-static approximation (5), which were in good agreement with the analytical solution (7) for a few cases.

While most afterslip generally occurs below or above the seismogenic zone [Marone *et al.*, 1991; Hsu *et al.*, 2006], there are observations suggesting that afterslip can also occur along strike the rupture zone [Melbourne *et al.*, 2002; Pritchard and Simons, 2006; Chlieh *et al.*, 2007], or even within the rupture area [Miyazaki *et al.*, 2004], and can be associated with aftershocks [Miyazaki *et al.*, 2004]. To explain these observations within the steady state approximation, we need to invoke small scale spatial or temporal variations of the friction parameters  $A$  or  $B$  [Miyazaki *et al.*, 2004; Wennerberg and Sharp, 1997].

Miyazaki *et al.* [2004] attempted to distinguish between velocity-weakening and velocity strengthening behavior for different parts of the fault that slipped after the 2003 Tokachi-oki earthquake. They inverted afterslip and stress changes on the fault from GPS data. They found that, within the rupture area, slip rate and stress initially decrease with time. But then stress increases while slip velocity continues to decrease. For other parts of the fault around the rupture area, stress decreases roughly linearly with the log of the slip rate, as expected with the steady state approximation (5). Miyazaki *et al.* [2004] interpreted these results as evidence for velocity-weakening (unstable) behavior within the rupture area, and velocity-strengthening regime around the mainshock rupture. However, the steady state approximation (5) is only valid at constant slip speed, while slip rate changes by several orders of magnitude in their observations. The different behavior between the rupture area and surrounding regions may rather arise from different stress histories: stress increases within the rupture area because it is reloaded by surrounding region, where afterslip is larger.

Marone *et al.* [1991] also evoked the possibility that afterslip may be produced by unstable faults, but noted that "for a fault that exhibits only velocity-weakening behavior, the steady-state frictional resistance decreases with slip velocity, eliminating the stress transient needed to drive afterslip." However, it is possible to produce significant afterslip starting from the steady state with  $B > A$ , and with realistic values of  $D_c$ . Rice and Tse [1986] studied a simple slider-block model in the unstable regime including inertia, and showed that the slider is close to steady state during inertia controlled instability, when slip exceeds  $D_c$ . During dynamic rupture, stress first decreases as slip velocity increases, but

further increases as slip decelerates. When inertia becomes negligible, the system escapes from the steady-state regime, and both slip rate and stress slowly decrease with time (see fig 3a of [Rice and Tse, 1986]). Thus, even if the slider is in the steady state regime at the end of dynamic rupture, there can be significant afterslip for velocity weakening faults. In addition, earthquake rupture is more complex than with single degree of freedom systems. There may be parts of the fault where slip is smaller than  $D_c$ , and stress transfers during dynamic rupture propagation can produce stress concentration, so that stress can be locally larger than its steady state value after a mainshock.

In this section, we study analytically and numerically the complete rate-and-state friction law (1,2) both in the velocity-strengthening and in the velocity-weakening regimes. We then attempt to invert the friction law parameters by fitting the afterslip data of Wennerberg and Sharp [1997] for the 1987 Superstition Hills earthquake.

### 2.3. Stability condition

Depending on the parameter  $B/A$ , stiffness  $k/k_c$ , and stress, the system exhibits either decaying afterslip, slow earthquakes, or slip singularity ("aftershock"). Rice and Tse [1986] derived the condition of stability for a slider without loading rate ( $\dot{\tau}_r = 0$ ) with  $B > A$  and  $k < k_c$ . They found that the system is stable if  $\mu < \mu_i$  with

$$\mu_i(V) = \mu_{ss}(V) + \frac{kD_cB}{(B-A)\sigma} = \mu_{ss}(V) + \frac{kB}{k_c} \quad (11)$$

We compute below the limit of the friction coefficient above which initial acceleration is positive. We rewrite the rate-and-state friction law (1) and (3) as

$$V = V_0 e^{-k\delta/A\sigma} \left( \frac{\theta}{\theta_0} \right)^{-B/A} \quad (12)$$

where  $V_0$  and  $\theta_0$  are the initial values of  $V$  and  $\theta$  respectively. Taking the time derivative of (12), acceleration of the slider is given by

$$\dot{V} = V \left( -\frac{kV}{A\sigma} - \frac{B\dot{\theta}}{A\theta} \right). \quad (13)$$

Thus slip accelerates if  $\dot{\theta} < -kV\theta/\sigma B$ . Using the state evolution law (2), we get the limit value for the state rate

$$\dot{\theta} = \frac{1}{1 - B\sigma/kD_c} = \frac{1}{1 - k_c/(k(1 - A/B))} \quad (14)$$

We can rewrite eqs (1,2,5) to get a relation between friction and state rate

$$\mu = \mu_{ss}(V) + B \ln(1 - \dot{\theta}) \quad (15)$$

which gives the value of the friction  $\mu_a$  corresponding to  $\dot{V} = 0$

$$\mu_a(V) = \mu_{ss}(V) + B \ln \left( \frac{1}{1 - (1 - A/B)k/k_c} \right) \quad (16)$$

If both  $V$  and  $\dot{\theta}$  increase, the slider will eventually decelerate before reaching slip instability. For the system to reach instability, we need both  $\dot{V} > 0$ ,  $\dot{\theta} < 0$  and  $\dot{\theta} < 0$  (this is what we observe in the numerical simulations). The state acceleration is given by (taking the time derivative of (2), and using expression (13) of  $\dot{V}$ , and expression (2) of  $\dot{\theta}$ )

$$\ddot{\theta} = \frac{-\dot{\theta}V - \theta\dot{V}}{D_c} = \frac{\dot{\theta}V}{D_c} \left( \frac{B}{A} - 1 - \frac{kD_c}{A\sigma} \right) + \frac{kV}{A\sigma} \quad (17)$$

The system is thus unstable if  $\dot{\theta} < 0$ , which gives  $\dot{\theta} < 1/(1 - k_c/k)$  and yields another expression for the friction coefficient  $\mu_l$  at the stability limit

$$\mu_l(V) = \mu_{ss}(V) + B \ln \left( \frac{1}{1 - k/k_c} \right) \quad (18)$$

Slip instabilities can occur only when both  $B > A$  and  $k < k_c$ ; otherwise we can't have both  $\dot{\theta} < 0$  and  $\dot{\theta} < 0$ . The friction at the stability limit (18) is close to but larger than the condition for initial acceleration (16) of the slider. Between these two values, there is thus a range of parameters for which we observe "slow earthquakes", followed by a classic afterslip relaxation, in both the velocity strengthening or velocity weakening regimes. This behavior is similar to the observation by *Pritchard and Simons* [2006] of a slow slip event triggered by the 1995  $m_W = 8.1$  Chile earthquake.

## 2.4. Analytical study

We have performed numerical simulations and analytical study of the slider block model with a fixed loading point ( $\dot{\tau}_r = 0$ ). We found different regimes for which the model exhibits afterslip, with a slip rate decreasing approximately as a power-law of time. If initial stress is large enough, and for special values of the model parameters, the system exhibits slow earthquakes or aftershocks. The analytical calculations are shown in appendix A, while the main results are presented in Table 1. Figure 1 illustrates the different regimes as a function of  $B/A$  and  $k/|k_c|$ . The other parameter that controls the behavior of the slider is initial stress. The influence of initial stress is illustrated in Figure 2 for  $k/|k_c| = 0.8$  and in Figure 3 for  $k/|k_c| = 2.5$ . Figure 4 shows the temporal evolution of velocity, state variable, and friction, for numerical simulations with (top plots)  $B/A = 1.5$  and  $k = 0.8k_c$ , and (bottom plots)  $B/A = 0.5$  and  $k = 2.5|k_c|$ . Each curve corresponds to a different value of initial friction.

### 2.4.1. Slip and slip rate

We have found several solutions for the slip rate of the form

$$V = \frac{V_0}{(1 + t/t^*)^p}, \quad (19)$$

where the exponent  $p$  is either smaller, equal or greater than 1 depending on the model parameters, and  $t^*$  is a characteristic time, which depends on the initial conditions and on the friction law parameters. Generally, the system evolves from one regime to another one with time, so that the apparent exponent  $p = d \ln V / d \ln t$  can either increase or decrease with time.

In all cases with slip rate decaying with time, displacement is proportional to  $D_c$ . Depending on model parameters  $B/A$ ,  $k/|k_c|$ , and initial friction, total slip can be either much smaller or larger than  $D_c$ . In the first regime, as  $\delta$  becomes of the order of  $D_c$ , the system evolves from regime #1 to #4 if  $A > B$ , or from #1 to #6 if  $A < B$ . The regimes #5 and #6 require slip to be much smaller than  $A\sigma/k$ . If  $A > B$ , slip will eventually become larger than  $A\sigma/k$ , and the system will evolve from regime #5 to #4.

If  $B > A$ , slip in regime #6 increases much slower with time, and reaches a constant value at infinite times. There is thus no transition to another regime. If  $B \approx A$  and  $\dot{\theta}_0 \ll 1$ , then total afterslip on seismogenic faults (with  $k < k_c$ ) can be much larger than  $D_c$ .

When there is a transition to another regime, analytical solutions in Table 1 have to be modified by replacing the initial values  $\theta_0$ ,  $V_0$ , and  $\mu_0$  by their values at the time the system enters the new regime, and the slip produced previously has to be added to the solution for  $\delta$  and  $\mu$ .

In the unstable regime, for  $k < k_c$  and  $B > A$ , the system will eventually reach regime #6 if  $\mu_0 < \mu_l$ , otherwise it produces a slip instability (aftershock).

### 2.4.2. Characteristic times

In all cases, characteristic times  $t^*$  for afterslip are inversely proportional to initial slip rate: the faster it slips, the faster slip rate decays with time. The other parameters that controls  $t^*$  are friction parameters  $B/A$ , stiffness  $k/|k_c|$ ,  $D_c$ , and, for cases #5 and #6, the initial friction or state rate.

### 2.4.3. State and state rate

In the velocity strengthening regime  $A > B$ , state rate evolves toward  $\theta_l = 1/(1 - k_c/k)$ . Because  $k_c < 0$  when  $A > B$ , the asymptotic value of the state rate is in the range  $0 < \theta_l < 1$ . Thus, except for the special case  $k = k_c$ , the system never reaches the steady-state regime  $\dot{\theta} = 0$ . Decrease in velocity with time in the evolution law (2) has to be balanced by an increase in state and/or state rate. Therefore, the steady state regime  $\dot{\theta} = 0$  can be reached only at constant slip rate. We consider the load point is fixed. Thus slider velocity cannot evolve toward a positive fixed value, and the slider never stays in the steady state. In the velocity weakening regime  $A < B$ , state rate either decreases toward  $-\infty$  if  $\mu_0 > \mu_l(V_0)$ , or increases toward 1 if  $\mu_0 < \mu_l(V_0)$ . The steady state approximation  $\dot{\theta} \approx 0$  is thus valid only for  $A > B$  and  $k \ll k_c$ .

### 2.4.4. Friction

Friction during afterslip always decreases with time in the absence of an external loading ( $\dot{\tau}_r = 0$ ), because  $\mu = \mu_0 - k\delta/\sigma$ . Thus even in the "velocity strengthening regime", friction decreases with slip rate if slip rate decreases with time, while steady-state friction  $\mu_{ss}(V)$  increases with  $V$ . Change in friction with  $\ln V$  is different among the afterslip regimes in Table 1. The slope of  $\mu$  as a function of  $\ln V$  is  $A + qB$  in cases #1-3,  $A - B$  in case #4 (with  $A > B$ ), while friction is almost independent of  $\ln V$  in cases #5 and #6.

### 2.4.5. Slow earthquakes

If initial friction is larger than the condition for initial acceleration, and lower than the stability criteria (or in the stable regime  $A > B$ ), velocity first increases, without reaching seismic slip velocities. The slip speed then decreases as a power-law of time, following the regime #4 if  $A > B$ , or #6 if  $A < B$ . The maximum slip rate occurs at times of the order of  $t_l^*$ . If  $B > A$ , and if initial friction is  $\mu_{ss}(V_0) < \mu_0 < \mu_a(V_0)$ , there is a transient phase in which velocity is almost constant, and healing rate  $\dot{\theta}$  increases. This phase can produce aseismic slip larger than  $D_c$ , before the system evolves to regime #6 when  $\dot{\theta} \approx 1$ , and slip saturates.

## 2.5. Comparison with observations

Several studies have attempted to measure  $A$  or  $A - B$ , and to distinguish between the stable and unstable regimes from the evolution of stress with slip rate during afterslip. *Miyazaki et al.* [2004] have mapped the coseismic and post-seismic slip produced by the 2003 Tokachi-oki earthquake, as well as the change in shear stress on the fault, by inverting GPS time series. Most afterslip occurred around the rupture area, mostly downdip. Within these zones, the stress-velocity paths approximately follow  $d\tau/d\ln(v) = 0.6$  MPa. They interpret this result as an evidence that the main afterslip regions are velocity strengthening. Following *Marone et al.* [1991], they assume that stress is equal to its steady state value, and suggest that  $(A - B)\sigma = 0.6$  MPa. According to our analysis, this result would be true if the system was in the afterslip regime #4, but we cannot exclude the first regime in Table 1. In this case the slope  $d\tau/d\ln(v) = 0.6$  would be equal to  $A + qB$  instead of  $A - B$ , and we cannot distinguish between the velocity weakening

or strengthening regimes. We can only exclude the unstable case  $B > A$  and  $k < k_c$ , which never produces a linear decrease of  $\mu$  with  $\ln V$ .

It is difficult to explain with the interpretation of *Miyazaki et al.* [2004] why numerous aftershocks occurred in the areas of large afterslip, because aftershocks cannot nucleate within zones with  $A > B$ . *Miyazaki et al.* [2004] suggest small-scale variations in friction parameters  $A$  and  $B$  within the afterslip areas in order to explain the spatial distribution of aftershocks.

*Miyazaki et al.* [2004] also found significant afterslip within the rupture area, but with less slip than the surrounding zones, of the order of 0.1 m instead of 0.5 m downdip of the rupture zone. In this zone, stress decreases a little at short times, and then reloads, because afterslip is larger in the surrounding areas. They suggest that this behavior is similar to that of a single degree of freedom slider block model with a constant loading rate in the velocity weakening regime.

*Hsu et al.* [2006] apply the same method to the 2005 Nias earthquake, and obtain similar result. They use a simplified form of the rate-and-state friction law (1) with  $B = 0$  [*Perfettini and Avouac*, 2004], i.e., neglecting healing. They observe extensive afterslip up-dip from the main shock and a lack of substantial overlap between seismogenic and aseismic regions. Aftershock zones correspond to the transition between regions of coseismic and aseismic slip. In the regions of large afterslip, stress decreases roughly linearly with  $\ln(V)$ , with a slope  $d\tau/d\ln(v) \approx 0.2$  MPa at short times, but much smaller for times larger than 100 days. In the areas of smaller afterslip, shear stress increases a little with time, because these zones are reloaded by surrounding slipping areas. *Hsu et al.* [2006] nevertheless measure  $A\sigma$  from the slope  $d\tau/d\ln(v) \approx -0.02$  MPa, giving unphysical negative values for  $A$ .

## 2.6. Fitting afterslip data with the rate-and-state model

We use the afterslip data of the 1987  $m_W 6.6$  Superstition Hills earthquake in Southern California analyzed by *Wennerberg and Sharp* [1997], as well as displacement data for a creep event on the same fault. High-quality horizontal and vertical afterslip data were obtained from repeated surveys of six quadrilaterals established on the Superstition Hills fault [*Sharp and Saxton*, 1989; *Sharp et al.*, 1989]. The quads were distributed along approximately 20 km of the fault, from North to South referred to as N, NC, SC, SSC, FSSC, and S (see Fig 1 of [*Wennerberg and Sharp*, 1997]). For each station, we have 2 measurements of horizontal strike-slip displacement across the fault (labeled as " $h, S$ " and " $h, W$ " in Table 2), and one measure of vertical displacement (indicated by a subscript  $v$  in Table 2). Stations N, NC, SC and S were installed before the earthquake. The other quadrilaterals SSC and FSSC were established 91 days after the mainshock, and at these sites the later data were combined with earlier lower-resolution measurements of offset natural features. *Wennerberg and Sharp* [1997] also analyzed slip measurements of [*Bilham and Behr*, 1992] from a digital creepmeter a few hundred meters to the North of the FSSC quad (labeled as " $FSSC_{h,BB}$ " in Table 2). Following *Wennerberg and Sharp* [1997], we analyze the vertical time series only from the two quads S and SC, because vertical motions from the other quads are too small. Slip resolution is about 1 mm for afterslip data, and 0.001 mm for the creep event. But fit residuals of *Wennerberg and Sharp* [1997] are largely controlled by steps ("creep events"), whose amplitude can be as large as 7 mm.

*Wennerberg and Sharp* [1997] modeled the afterslip measurements using an alternative form of the rate-and-state friction law (1)

$$\mu = \frac{1 + B \ln(1 + \theta V^*/D_c)}{1 + A \ln(1 + V/V^*)} \quad (20)$$

and assuming steady-state behavior  $\dot{\theta} \approx 0$ . This friction law provided a better fit of afterslip data than the steady-state friction law (5) derived by *Scholz* [1990]. In particular, *Wennerberg and Sharp* [1997] found that slip velocity was decaying as a power law of time (19) with an exponent  $p = 1/(1 + B - A)$  [*Wesson*, 1988]. This model is thus able to explain why  $p$  values in Table 2 are often larger than 1. But it requires a very large value of  $A - B = 0.29$  in order to reproduce the value  $p = 1.29$  observed for afterslip at point  $S_{z,s}$ .

For one dataset, this model provided unphysical negative values for  $A$ , corresponding to an instantaneous decrease in friction following an increase in slip rate. Such a behavior has never been observed experimentally. For the other stations,  $A$  is ranging between 0.03 and 0.36, a bit larger than the values  $A \approx 0.01$  commonly observed in laboratory experiments [*Dieterich*, 1994]. *Wennerberg and Sharp* [1997] inverted for 4 model parameters and 1 initial condition. Comparison of model parameters obtained for different data sets (2 horizontal slip data  $S$  and  $W$  at each station, or using different time intervals) suggests that the inverted parameters are relatively well constrained.

In contrast with previous studies [*Marone et al.*, 1991; *Marone*, 1998; *Wennerberg and Sharp*, 1997; *Schaff et al.*, 1998; *Miyazaki et al.*, 2004; *Montési*, 2004; *Perfettini and Avouac*, 2004; *Hsu et al.*, 2006], we use the complete rate-and-state friction law instead of the steady-state approximation. We do not fit directly the displacement data, but the fits to the afterslip data obtained by *Wennerberg and Sharp* [1997] (see equation (18) and Table 1 of [*Wennerberg and Sharp*, 1997]), which fit the data with residuals of the order of the measurement resolution. We invert for 6 parameters (instead of 5 in [*Wennerberg and Sharp*, 1997]) :  $A$ ,  $B$ ,  $D_c$ ,  $k$ ,  $V_0$  and  $\mu_0$ . We use a Nelder-Mead algorithm to perform the nonlinear minimization of the slip residuals, using a large range of initial values for the inverted parameters. Specifically, the initial model parameters have random values determined by  $A = 0.01 \times 10^{2r_A}$ ,  $B = A(1 + r_B/2)$ ,  $V_0 = V_{d,0}(1 + r_V/2)$ ,  $D_c = 0.1 \times 10^{2r_{D_c}}$ ,  $k = A\sigma \times 10^{r_k}/D_c$  and  $\mu_0 = r_\mu$ , where  $r_A$ ,  $r_B$ ,  $r_{D_c}$ ,  $r_k$  and  $r_V$  are chosen according to a gaussian distribution of zero mean and standard deviation equal to 1,  $r_\mu$  is uniformly distributed between 0 and 1, and  $V_{d,0}$  is the initial velocity determined by *Wennerberg and Sharp* [1997]. For each data set, we have tested more than 100 initial models. We thus have a good sampling of the range of realistic model parameters.

Observed slip velocity is found to decrease with time approximately as  $V = V_0/(t/t^* + 1)^p$  with a characteristic time  $t^*$  of the orders of days, and an exponent  $p$  ranging between 0.88 and 1.3. (see values in Table 2). Figure 5 shows the "observed" slip rate (computed from the fit of *Wennerberg and Sharp* [1997]) and all our fits with the complete rate-state friction law with a residue smaller than 1 mm, for the data set  $S_{h,s}$  (line 12 in Table 12). A simple fit with  $V = V_0/(t/t^* + 1)^p$ , i.e., only 3 parameters, already provides a very good fit to the observations, with a residue of 0.5 mm. This makes it difficult to invert reliably for the 6 parameters of the rate-and-state law. Indeed, we find that there is a huge range of model parameters that fit the data within the measurement resolution. The inverted parameters appear to be mostly constrained by our choice of initial values in the optimization. Therefore, we did not report the inverted model parameters in Table 2. In particular, for most data sets we cannot distinguish between the velocity weakening and velocity strengthening regimes, and we can fit the data as well with  $k < k_c$  or  $k > k_c$ . Only the horizontal slip data of the  $N$  quad requires  $A > B$ . This is the

only station that has an exponent  $p < 1$ . Such a behavior cannot be reproduced with  $A < B$  (except over a limited time interval). The *FSSC* quad produces different results for independent slip measurements at points separated by a few meters. For the creep event, all models that fit the data are in the velocity weakening regime with  $k > k_c$ .

The critical slip distance inverted from the data ranges from a few  $\mu\text{m}$  to several km, most of the time comparable to the initial value used in the optimization. Total afterslip (of the order tens of centimeter) can thus be much larger or smaller than  $D_c$ . Even for seismogenic faults, with  $B > A$  and  $k < k_c$ , we found models that fitted the data with  $D_c$  as small as 1% of the maximum afterslip.

### 3. Seismicity rate triggered by afterslip

#### 3.1. Relation between stress and seismicity

Previous studies [Dieterich, 1994; Schaff *et al.*, 1998] have already suggested that afterslip can trigger aftershocks by reloading parts of the fault that are locked after the mainshock. Most studies who suggested that aftershocks are due to afterslip assumed that aftershock rate is simply proportional to stress or strain rate [Wennerberg and Sharp, 1997; Schaff *et al.*, 1998; Perfettini and Avouac, 2004; Hsu *et al.*, 2006]. However, Dieterich [1994] showed that the relation between seismicity rate and stress rate can be much more complex. For instance, in the case of a simple stress step  $\Delta\tau$  followed by a constant stressing rate  $\dot{\tau}_r$ , the seismicity rate  $R(t)$  is given by [Dieterich, 1994]

$$R(t) = \frac{r}{(e^{-\Delta\tau/A\sigma} - 1)e^{-t/t_a} + 1}, \quad (21)$$

where  $t_a = A\sigma_n/\dot{\tau}_r$  is the duration of the nucleation phase of an earthquake, and is also equal to the duration of an aftershock sequence.  $r$  is the seismicity rate for a constant stressing rate equal to  $\dot{\tau}_r$ . Aftershock rate increases immediately after the stress step, and then decreases with time back to  $R = r$  for  $t \gg t_a$ . Typically,  $t_a$  is of the order of years [Dieterich, 1994]. This shows that there can be a very long time delay between a change in stress and triggered seismicity. The assumption that aftershock rate is proportional to stress rate for earthquakes triggered by afterslip thus needs to be verified.

Dieterich [1994] derived a general relation between stress rate and seismicity rate, which we use to model seismicity triggered by afterslip

$$R = \frac{r}{\gamma \dot{\tau}_r} \quad (22)$$

where  $\gamma$  is a seismicity state variable, which evolves as

$$\dot{\gamma} = \frac{1}{A\sigma}(1 - \gamma\dot{\tau}) \quad (23)$$

We can rewrite (23) as

$$\frac{-A\sigma\dot{\gamma} + 1}{\gamma} = \dot{\tau}. \quad (24)$$

Integrating (24) and using the definition (22), we get a simple form for the relation between seismicity rate  $R$ , cumulative number of events  $N = \int_0^t R dt$ , and stress change  $\tau = \int_0^t \dot{\tau} dt$

$$A\sigma \ln\left(\frac{R}{R_0}\right) + \frac{N\dot{\tau}_r}{r} = \tau. \quad (25)$$

For  $R$  changing slowly in time, we can neglect the first term in (25). So the seismicity rate is proportional to the

stressing rate, specifically

$$R = \frac{r\dot{\tau}}{\dot{\tau}_r} \quad (26)$$

For rapid variations of seismicity rate, we can neglect the second term in (25). The seismicity rate thus increases exponentially with stress

$$R = R_0 \exp(\tau/A\sigma) \quad (27)$$

Beeler and Lockner [2003] measured the correlation between seismicity rate and stress in laboratory friction experiments, with a periodic perturbation of the stress rate superposed to a constant loading rate. They found that the relation between seismicity rate and stress is in good agreement with expression (26) for slow stress changes, and with equation (27) for fast stress changes. Expression (27) also provides a good fit to seismicity triggered by tides [Cochran *et al.*, 2004], though the small values of the stress change  $\tau/A\sigma$  do not allow to test if  $R$  increases proportionally or exponentially with  $\tau$ .

#### 3.2. Application to model seismicity triggered by afterslip

##### Stress rate

We have shown previously that slip rate in the rate and state model can be modeled by a power law decay  $V = V_0/(1 + t/t^*)^p$ , with a characteristic time  $t^*$ , and an exponent  $p$  that depend on the friction law parameters  $B/A$  and  $k/k_c$ , and on the initial conditions  $V_0$  and  $\mu_0$ . Initial slip rate and friction are likely to be very heterogeneous, due to variations of coseismic slip. As a consequence, areas of the fault that are approximately locked after the mainshock (small  $V_0$ ) will be reloaded by adjacent areas with larger slip rate. Using our simple slider-block model, we can model the stress rate induced by afterslip as

$$\dot{\tau} = kV = \frac{kV_0}{(1 + t/t^*)^p} \quad (28)$$

where  $V$  represents the difference in slip rate between "locked" and "slipping" parts of the fault.

##### Special case $p = 1$

There is an analytical solution to equation (23) with stress following (28) only for the special case  $p = 1$ , which is given by

$$R = \frac{r}{\dot{\tau}_r} \left[ C(1 + t/t^*)^{-n} + \frac{1 + t/t^*}{\dot{\tau}_0(1 + 1/n)} \right]^{-1}, \quad (29)$$

where  $C$  is a constant given by, assuming initial seismicity rate equals  $r$ ,

$$C = \frac{1}{\dot{\tau}_r} - \frac{1}{\dot{\tau}_0(1 + 1/n)}, \quad (30)$$

$n$  is defined by

$$n = \dot{\tau}_0 t^*/A\sigma, \quad (31)$$

$\dot{\tau}_0 = kV_0$  is initial stress rate. For large stress rate, the second term is negligible in (30) and  $C \approx 1/\dot{\tau}_r$ .

In this case  $p = 1$ , the seismicity rate first increases with time and reaches its maximum value for time equal to

$$t_{R_{\max}} = t^* \left[ (C\dot{\tau}_0(n + 1))^{1/(n+1)} - 1 \right]. \quad (32)$$

As stress change increases,  $t_{R_{\max}}$  decreases. For times larger than  $t_{R_{\max}}$ , seismicity rate predicted by (29) decreases pro-

portionally to the stress rate

$$R \approx \left(1 + \frac{1}{n}\right) \frac{r\dot{\tau}}{\dot{\tau}_r}. \quad (33)$$

For large  $n$  (large stress rate), expression (33) recovers expression (26) for the stress-seismicity relation that is valid for slowly varying  $R$ .

### General case $p \neq 1$

For  $p \neq 1$ , we found numerically that expression (33) is still a rather good approximation of the time  $t_{R_{\max}}$  at which  $R$  reaches its maximum. At intermediate times  $t > t_{R_{\max}}$  expression (33) also provides a good fit to the seismicity rate, i.e., seismicity rate is proportional to stress rate. However, if  $p > 1$ , we found in numerical simulations of (25) that there is a characteristic time  $t_c$  after which expression (33) does not hold. Typical evolutions of seismicity rate and stress rate are shown in Figure 6 for  $p = 1.3$  and in Figure 7 for  $p = 0.8$ .

If  $p > 1$ , stress and thus number of events  $N$  will saturate for  $t \gg t^*$ . The stress change will increase toward a maximum value  $\Delta\tau$  given by

$$\Delta\tau = \int_0^\infty \dot{\tau} dt = \frac{\dot{\tau}_0 t^*}{p-1}. \quad (34)$$

The first term  $\sim \ln(R)$  will become non negligible compared with the term  $\sim N$  in (25). The seismicity rate for large times  $t \gg t^*$  and  $t \gg t_{R_{\max}}$  will thus be equivalent to that triggered by an instantaneous stress step of amplitude  $\Delta\tau$ , described by equation (21). The "long time seismicity rate", for  $t_c \ll t \ll t_a$ , evolves according to  $R \approx rA\sigma/t\dot{\tau}_r$  (assuming  $t_c \gg t_a \exp(-\Delta\tau/A\sigma)$ ).

The transition from the regime  $R \approx r\dot{\tau}/\dot{\tau}_r$  described by (33) for  $t_{R_{\max}} \ll t \ll t_c$  to the regime  $R \approx rA\sigma/t\dot{\tau}_r$  for  $t \gg t_c$  will occur at a time  $t_c$  given by  $\dot{\tau}(t_c) = A\sigma/t_c$ . Assuming  $t_c \gg t^*$ , we get

$$t_c = t^* n^{1/(p-1)}. \quad (35)$$

If there is a non-zero constant stress rate  $\dot{\tau}_r$ , in addition to the stress rate (28) induced by afterslip, seismicity rate decays as the inverse of time for  $t_c \ll t \ll t_a$ , until it reaches its background level  $r$ . The number of events triggered by afterslip can be computed directly from (25). When  $R$  returns to its initial value  $R_0 = r$  and  $\tau = \Delta\tau$ , the first term is equal to zero in (25) and  $N = r\Delta\tau/\dot{\tau}_r$ . This results is independent of the form of the stress change, as long as stress reaches a maximum value  $\Delta\tau$  at long times. The stress change needed to explain the observed number of aftershocks is thus the same for static triggering (stress step of amplitude  $\Delta\tau$ ), and for triggering due to afterslip.

For a slow decay of stress rate with time  $p < 1$ , which requires  $A > B$  (see Table 1), stress does not saturate for  $t \gg t^*$  but instead increases as  $\tau = \int_0^t \dot{\tau} dt \sim t^{1-p}$  for  $t \gg t^*$ . Seismicity rate thus never reaches the regime described by (21) with  $R \sim 1/t$ . In this case, seismicity rate is proportional to stress rate as predicted by (33) for  $t > t_{R_{\max}}$ .

This work shows that seismicity rate triggered by afterslip does not always scale with slip rate, as assumed by [Wennerberg and Sharp, 1997; Schaff et al., 1998; Perfettini and Avouac, 2004; Hsu et al., 2006]. For instance, we can observe  $V \sim \dot{\tau} \sim t^{-p}$  with  $p > 1$  but  $R \sim 1/t$ . The characteristic times  $t_{R_{\max}}$  and  $t_c$  that control seismicity rate are also different from the characteristic time  $t^*$  which controls afterslip rate.

### Comparison with aftershock data

Aftershock studies [Helmstetter et al., 2005; Peng et al., 2007] have shown that seismicity rate decreases with time

according to  $R \sim R_0/(1+t/c)^p$ , with a characteristic time  $c$  that is no larger than 10 sec, and an exponent  $p$  that can be either smaller or larger than 1, and is usually between 0.9 and 1.2 [Reasenber and Jones, 1994; Helmstetter et al., 2003]. Seismicity rate can increase by a factor up to  $10^5$  relative to the background rate. The duration of aftershock sequences is of the order of years, i.e., about  $10^6$  larger than the characteristic time  $c$ .

In order to explain aftershock triggering by afterslip, we need the characteristic times  $t^*$  to be of the order of seconds. This is much smaller than the values of  $t^*$  of a few days estimated for afterslip data following Superstition Hills earthquake [Wennerberg and Sharp, 1997] (see Table 2). However, afterslip was measured at the surface, we can expect strong fluctuations of  $t^*$  with depth due to changes of friction parameters or initial values.  $t^*$  may thus be much smaller at depth, where aftershocks nucleate.

Afterslip following the  $m_W = 8.7$  2005 Nias earthquake, and measured by GPS, also produces  $t^*$  of the order of 3 days [Hsu et al., 2006] for all GPS points. Hsu et al. [2006] found that both displacement and aftershock number increase logarithmically with time  $\sim \ln(1+t/t^*)$ , with  $t^* \approx 3$  days. However, they counted the number of  $m > 3$  aftershocks triggered by the mainshock, while the catalog is not complete for such small events, and the completeness level decreases with time after the mainshock. Using only  $m \geq 5.5$  aftershocks, we measured  $t^* \approx 0.1$  day, much smaller than the characteristic time of afterslip inferred from GPS measurements. It is thus unlikely that early aftershocks of the Nias earthquake are governed by afterslip.

As shown above, the stress change involved to trigger  $N$  events is the same for static triggering and for triggering by afterslip. Because the amplitude of afterslip is often comparable to coseismic slip [Pritchard and Simons, 2006], the number of events triggered by afterslip should be comparable to that triggered by coseismic stress change, in the unstable areas of the faults with  $B > A$  and  $k < k_c$ . If  $p \approx 1$ , or for static triggering, the stress change needed to produce an increase of seismicity rate by a factor  $10^5$  is  $\Delta\tau = A\sigma \ln(10^5) = 11.5A\sigma$ . If  $A\sigma \approx 0.1$  MPa, as suggested by Cochran et al. [2004], this gives realistic values, smaller than the average stress drop. On the other hand, if we use the laboratory value  $A \approx 0.01$  [Dieterich, 1994], and a normal stress  $\sigma = 100$  MPa (of the order of the lithostatic pressure at a depth of about 5 km), then the stress change needed is  $\Delta\tau = 11.5$  MPa. This seems quite large, however it is possible that maximum stress change can locally reach such values. As shown by Helmstetter and Shaw [2006], seismicity rate triggered by a heterogeneous stress change at short times is controlled by the maximum stress change rather than the mean value.

If we want to reproduce observations of seismicity rate decaying with  $p > 1$  over several decades in time, we need even larger stress change than for  $p \leq 1$ . For instance, following the 1992  $m_W 7.3$  Landers earthquake, the seismicity rate decreased with time as  $R \sim t^{-1.2}$  over 5 decades in time. To explain this pattern, we thus need  $t_c \geq 10^5 t_{R_{\max}}$ . We have computed the seismicity rate triggered by the stress change modeled by (28) with  $p = 1.2$ , using numerical integration of equation (25). We found that the stress change  $\Delta\tau$  defined by (34) required to get  $t_c \geq 10^5 t_{R_{\max}}$  is  $\Delta\tau \approx 50A\sigma$ .

## 4. Conclusion

We have modeled the postseismic slip of faults using the rate-and-state friction law. The postseismic behavior of faults is more complex than predicted previously based on the steady state approximation of the friction law. We found that, depending on the model parameters  $B/A$  and  $k/|k_c|$ , and on initial friction, the fault exhibits either decaying afterslip, slow earthquakes, or aftershocks. Afterslip, with

slip amplitude comparable or even larger than  $D_c$ , can be obtained for any value of the friction law parameters, even for velocity weakening faults ( $B > A$ ). We have derived several approximate solutions to describe the evolution of slip, state and friction with time. There are several regimes with different characteristic times  $t^*$  and exponents  $p$  for which afterslip decays according to  $V = V_0/(1 + t/t^*)^p$ . This expression of the slip rate provides a very good fit to afterslip data [Wennerberg and Sharp, 1997], with  $t^*$  of the order of days, and  $p$  ranging between 0.9 and 1.3. The number of parameters of the rate-and-state model is too large in order to invert from afterslip data. For most data sets we studied, afterslip can be modeled as well with velocity weakening or strengthening friction parameters. Therefore, we don't need to involve spatial or temporal changes in the friction law parameter  $B/A$  in order to explain the evolution between aseismic and seismic slip.

Aftershock decay with time (Omori law) is similar to that observed for afterslip rate. This similarity led several authors to suggest that aftershocks are induced by the postseismic reloading of the fault due to afterslip. Using the relation between stress and seismicity derived by Dieterich [1994], we have shown that afterslip is indeed a possible mechanism to explain aftershock triggering. But the relation between slip rate and seismicity rate is more complex than previously thought [Wennerberg and Sharp, 1997; Schaff et al., 1998; Perfettini and Avouac, 2004; Hsu et al., 2006]. The process of earthquake nucleation indeed introduces a time delay between stress change and triggered earthquakes. As a consequence, seismicity rate is characterized by exponents and characteristic times that can be different from those that control stress rate. The complexity of the friction law thus makes it difficult to infer the mechanisms responsible for earthquake triggering based on observations of stress changes. Moreover, we have simplified the problem by considering uniform values of the model parameters, and of the slip rate, by modeling the fault with a simple slider block with one degree of freedom. We have also neglected other processes that may play an important role in the evolution of faults, such as fluid flow, viscous deformation, dynamic stress changes, and subcritical crack growth, among other mechanisms, all of which could have their own time dependence. The modeling of fault slip and seismicity, and even more the characterization of the fault rheology based on seismicity or geodesy data, is thus a difficult challenge, in terms of finding which mechanism may be causing an observed time dependence. In this paper, we have added to this difficulty by demonstrating additional time dependent behavior in the primary candidate, the rate and state friction law.

**Acknowledgments.** Part of this work was done while the authors were at the KITP in Santa Barbara. This research was supported in part by the National Science Foundation under grants PHY99-0794 and EAR03-37226, and the Southern California Earthquake Center, and by European Commission under grant TRIGS-043251.

## Appendix A: Analytical study of afterslip

We first search for solutions to the rate-and-state friction law with slip rate decaying as the inverse of time

$$V(t) = \frac{V_0}{(1 + t/t^*)}. \quad (\text{A1})$$

Putting this solution into the rate-and-state law (1), we get

$$-\frac{kV_0t^*}{\sigma} \ln \left( 1 + \frac{t}{t^*} \right) = -A \ln \left( 1 + \frac{t}{t^*} \right) + B \ln \theta + \text{constant}. \quad (\text{A2})$$

The evolution law (2) becomes

$$\dot{\theta} = 1 - \frac{V_0}{D_c} \frac{\theta}{(1 + t/t^*)}, \quad (\text{A3})$$

whose solution is

$$\theta = K(t^* + t)^{-q} + \frac{t^* + t}{q + 1}, \quad (\text{A4})$$

where  $K$  is a constant and  $q = V_0t^*/D_c$ . Depending on time and model parameters, the first or the second term will dominate in (A4).

At short times, the first term dominates in (A4). Using this approximation, the friction law (A2) becomes

$$\left[ A + \frac{BV_0t^*}{D_c} - \frac{kV_0t^*}{\sigma} \right] \ln \left( 1 + \frac{t}{t^*} \right) = \text{constant}, \quad (\text{A5})$$

which implies that the characteristic time  $t^*$  in (A1) obeys

$$t^* = \frac{A}{kV_0/\sigma - BV_0/D_c} = \frac{D_c A/V_0}{(B - A)k/k_c - B}, \quad (\text{A6})$$

with  $k_c = (B - A)\sigma/D_c$ . Depending on  $B/A$  and  $k/k_c$ ,  $q$  and  $t^*$  can be either positive or negative. The expression of  $q$  as a function of  $B/A$  and  $k/|k_c|$  is thus

$$q = \frac{V_0t^*}{D_c} = \frac{A}{(B - A)k/k_c - B}, \quad (\text{A7})$$

and is shown in Figure 1.  $q$  is always negative in the unstable regime  $B > A$  and  $k < k_c$ , but can be either positive or negative if  $B < A$  or  $k > |k_c|$ .

When  $q > 0$ , the approximation  $K(t^* + t)^{-q} \ll (t^* + t)/(q + 1)$  in (A4) will hold as long as  $t \ll t_1 (D_c/\theta_0 V_0 (q + 1))^{-1/(1+q)}$ . This corresponds to regime #1 (see Table 1 for a list of regimes and approximations). If the system is initially close to steady state, i.e.,  $\dot{\theta}_0 \approx 0$ , then  $\theta_0 \approx D_c/V_0 = t^*/q$ . The transition to the next regime occurs at times of the order of  $\theta_0$ , when the slip is  $\delta \approx D_c q \ln(1 + 1/q) \approx D_c$ . The slip generated during this phase thus reaches a maximum value of the order of  $D_c$  before the transition to the next regime when the second term in (A4) dominates, which is regime #4 in Table 1.

If  $q < 0$ , then  $t^* < 0$  and equation (A1) describes a power-law singularity of slip rate (earthquake). In this case, we recover the solution derived by [Dieterich, 1994] for earthquake nucleation in the absence of external loading ( $\dot{\tau}_r = 0$ ). This solution is valid only for large stress  $\mu(V) > \mu_a(V)$ , i.e., when slip rate initially increases with time. This corresponds to regime #2 in Table 1. In addition, the system will not reach instability if  $\dot{\theta} > 0$ , corresponding to  $\mu(V) < \mu_l(V)$ . If  $\mu(V) < \mu_l(V)$ , fault healing accelerates, eventually forcing slip rate to decrease with time. This corresponds with the slow earthquake case, discussed in Section 2.4.5, of regime #2 transforming to regime #6, or regime #3 transforming to regime #4 or regime #6; see Figure 1.

The second term  $(t^* + t)/(q + 1)$  dominates at large times if  $q > 0$  and  $t^* > 0$ . Putting this approximate solution  $\theta = (t^* + t)/(q + 1)$  in (A2), this gives

$$\left[ A - B - \frac{k}{\sigma} V_0 t^* \right] \ln \left( 1 + \frac{t}{t^*} \right) = \text{constant}, \quad (\text{A8})$$

which implies

$$t^* = \frac{(A - B)\sigma}{kV_0}. \quad (\text{A9})$$

This characteristic time is the same as found by Scholz [1990] using the steady state approximation. The friction coefficient given by (1,A4) is  $\mu = \mu_0 + (A - B) \ln(V/V_0)$ , equal

to the steady-state value. However our solution (A1,A4) is not at steady state; healing rate given by (A3) is

$$\dot{\theta} = \frac{1}{1 + t^*V_0/D_c} = \frac{1}{1 - k_c/k}. \quad (\text{A10})$$

This corresponds to regime #4.

We also found another regime for which slip rate decays as a power of time, with an exponent  $B/A$ . This regime characterizes afterslip when  $\delta \ll A\sigma/k$ , i.e., when change in friction due to slip is negligible. With this approximation, slip rate (12) can be rewritten as

$$V = V_0 \left( \frac{\theta}{\theta_0} \right)^{-B/A} \quad (\text{A11})$$

and the evolution law (2) becomes

$$\dot{\theta} = 1 - \frac{V_0\theta_0}{D_c} \left( \frac{\theta}{\theta_0} \right)^{1-B/A} \quad (\text{A12})$$

This solution has no analytical solution. To obtain simple solutions, we further assume that either (i)  $B \approx A$ , so that  $\dot{\theta} \approx 1 - V_0\theta_0/D_c$ , or (ii) slip rate is small, so that  $\dot{\theta} \approx 1$ . State variable is thus given by  $\theta = \theta_0 + \dot{\theta}_0 t$ , and slip rate obeys

$$V = \frac{V_0}{(1 + \dot{\theta}_0 t/\theta_0)^{-B/A}}. \quad (\text{A13})$$

Our solution (A13) can be applied as well in the velocity weakening case, corresponding to regime #5, or velocity strengthening case, corresponding to regime #6. In the stable regime, the solution (A13) will be followed by the other power law decay described by (A1,A9), when slip becomes large compared with  $A\sigma/k$ .

## References

- Beeler N. M., D. A. Lockner (2003), Why earthquakes correlate weakly with the solid Earth tides: Effects of periodic stress on the rate and probability of earthquake occurrence, *J. Geophys. Res.*, 108 (B8), 2391, doi:10.1029/2001JB001518.
- Bilham, R., and Behr, J. (1992). A two-layer model for aseismic slip on the Superstition Hills fault, California. *Bull. Seismol. Soc. Am.* 82, 1223-1235.
- Chlieh, M., J.P. Avouac, V. Hjorleifsdottir, T.A. Song, C. Ji, K. Sieh, A. Sladen, H. Hebert, L. Prawirodirdjo, Y. Bock, and J. Galetzka (2007), Coseismic slip and afterslip of the Great  $M_w$  9.15 Sumatra-Andaman Earthquake of 2004, *Bull. Seism. Soc. Am.* 97, doi: 10.1785/0120050631.
- Cochran, E. S., J. E. Vidale and S. Tanaka (2004) Earth tides can trigger shallow thrust fault earthquakes, *Science* 306, 1164-1166.
- Dieterich, J. H. (1979), Modeling of rock friction, 1. Experimental results and constitutive equations. *J. Geophys. Res.* 84, 2161-2168.
- Dieterich, J. H. (1994), A constitutive law for the rate of earthquake production and its application to earthquake clustering, *J. Geophys. Res.*, 99, 2601.
- Dieterich, J. H., V. Cayol and P. Okubo (2000), The use of earthquake rate as a stress meter at Kilauea volcano, *Nature* 408, 457-460.
- Freed A. M., R. Bürgmann, E. Calais, J. Freymueller, S. Hreinsdóttir (2006), Implications of deformation following the 2002 Denali, Alaska, earthquake for postseismic relaxation processes and lithospheric rheology, *J. Geophys. Res.*, 111, B01401, doi:10.1029/2005JB003894
- Gomberg, J., N. M. Beeler, M. L. Blanpied, and P. Bodin (1998), Earthquake triggering by transient and static deformation, *J. Geophys. Res.*, 103, 24,411-24,426.
- Heki, K., S. Miyazaki, and H. Tsuji (1997), Silent fault slip following an interplate thrust earthquake at the Japan Trench, *Nature*, 386, 595-598.
- Helmstetter, A., G. Ouillon and D. Sornette (2003), Are aftershocks of large californian earthquakes diffusing? *J. Geophys. Res.*, 108, 2483, 10.1029/2003JB002503.
- Helmstetter, A., Y. Kagan and D. Jackson (2005), Importance of small earthquakes for stress transfers and earthquake triggering, *J. Geophys. Res.* 110, B05S08, 10.1029/2004JB003286.
- Helmstetter, A., and B. E. Shaw, Estimating stress heterogeneity from aftershock rate, *J. Geophys. Res.*, *in press*, 2006.
- Hsu, Y.-J., M. Simons, J.-P. Avouac, J. Galetzka, K. Sieh, M. Chlieh, D. Natawidjaja, L. Prawirodirdjo, and Y. Bock (2006), Frictional afterslip following the 2005 Nias-Simeulue earthquake, Sumatra, *Science* 312, 1921-1926, DOI: 10.1126/science.1126960
- Marone, C.J., Scholz, C.H. and R. Bilham (2006), On the mechanics of earthquake afterslip, *J. Geophys. Res.* 111, B06305.
- Marone, C. (1998), Laboratory-derived friction laws and their application to seismic faulting. *Ann. Revs. Earth & Plan. Sci.*, 26, 643-696.
- Marsan, D. (2006), Can co-seismic stress variability suppress seismicity shadows? Insights from a rate-and-state friction model, *J. Geophys. Res.* 111, B06305, doi:10.1029/2005JB004060.
- Melbourne, T., F. Webb, J. Stock, and C. Reigber (2002), Rapid postseismic transients in subduction zones from continuous GPS, *J. Geophys. Res.*, 107(B10), 2241, doi:10.1029/2001JB000555.
- Miyazaki S., P. Segall, J. Fukuda, T. Kato (2004), Space time distribution of afterslip following the 2003 Tokachi-oki earthquake: Implications for variations in fault zone frictional properties, *Geophys. Res. Lett.*, 31, L06623, doi:10.1029/2003GL019410.
- Montési, L. G. J. (2004), Controls of shear zone rheology and tectonic loading on postseismic creep, *J. Geophys. Res.*, 109, B10404, doi:10.1029/2003JB002925.
- Nur, A., and J. R. Booker (1972), Aftershocks caused by pore fluid flow?, *Science*, 175, 885.
- Nur, A., and G. Mavko (1974), Postseismic viscoelastic rebound, *Science* 18, 204-206, DOI: 10.1126/science.183.4121.204
- Peng, Z., J.E. Vidale, M. Ishii and A. Helmstetter (2007), Anomalous seismicity rate immediately before and after mainshock rupture from high-frequency waveforms in Japan, *in press* in *J. Geophys. Res.*
- Perfettini H., J.-P. Avouac (2004), Postseismic relaxation driven by brittle creep: A possible mechanism to reconcile geodetic measurements and the decay rate of aftershocks, application to the Chi-Chi earthquake, Taiwan, *J. Geophys. Res.*, 109, B02304, doi:10.1029/2003JB002488.
- Pollitz, F. F., M. Nyst, T. Nishimura, and W. Thatcher (2006), Inference of postseismic deformation mechanisms of the 1923 Kanto earthquake, *J. Geophys. Res.*, 111, B05408, doi:10.1029/2005JB003901.
- Pritchard, M. E., and M. Simons (2006), An aseismic slip pulse in northern Chile and along-strike variations in seismogenic behavior, *J. Geophys. Res.*, 111, B08405, doi:10.1029/2006JB004258
- Reasenber, P. A., and Jones, L. M. (1994), Earthquake aftershocks: update, *Science*, 265, 1251-1252.
- Rice, J. R. and S. T. Tse (1986), Dynamic motion of a single degree of freedom system following a rate and state dependent friction law, *J. Geophys. Res.* 91, 521-530.
- Ruina, A. (1983), Slip instability and state variable friction laws. *J. Geophys. Res.* 88, 10359-10370.
- Schaff, D. P., G. C. Beroza, and B. E. Shaw (1998), Postseismic response of repeating aftershocks, *Geophys. Res. Lett.*, 25, 4549.
- Scholz, C.H., (1990) *The mechanics of earthquake and faulting*, Cambridge University Press, new York.
- Segall, P., E. Desmarais, D. Shelly, A. Miklius, and P. Cervelli (2006), Earthquakes triggered by silent slip events on Kilauea volcano, Hawaii, *Nature*, 442.
- Sharp, R.V., Saxton, J.L. (1989). Three-dimensional records of surface displacement on the Superstition Hills fault zone associated with the earthquakes of 24 November 1987. *Bull. Seismol. Soc. Am.* 79, 376-389.

- Sharp, R.V., Budding, K.E., Boatwright, J., Ader, M.J., Bonilla, M.G., Clark, M.M., Fumal, T.E., Harms, K.K., Lienkaemper, J.J., Morton, D.M., O'Neill, B.J., Ostergren, C.L., Ponti, D.J., Rymer, M.J., Saxton, J.L., Sims, J.D. (1989). Surface faulting along the Superstition Hills fault zone and nearby faults associated with the earthquakes of 24 November 1987. *Bull. Seismol. Soc. Am.* 79, 252-281.
- Takai, K., H. Kumagai, N. Fujii (1999), Evidence for slow slip following a moderate-size earthquake (Mw=5.7) in a subducting plate, *Geophys. Res. Lett.*, 26(14), 2113-2116, 10.1029/1999GL900465.
- Wennerberg, L. and R. V. Sharp (1997) Bulk friction modeling of afterslip and the modified Omori law, *Tectonophysics* 277, 109-136.
- Wesson, R L (1988) Dynamics of fault creep, *J. Geophys. Res.*, 93(B8), 8929-8951, doi:10.1029/88JB00134.
- Yoshida, S., and N.Kato (2003), Episodic aseismic slip in a two-degree-of-freedom block-spring model , *Geophys. Res. Lett.* 30,1681, doi:10.1029/2003GL017439
- 
- Agnès Helmstetter, LGIT, Maison des Géosciences, BP 53, 38041 Grenoble Cedex 9 , France (e-mail: ahelmste@obs.ujf-grenoble.fr)
- Bruce Shaw, Lamont-Doherty Earth Observatory, 61 Rte 9W, Palisades, NY 10964 (e-mail: shaw@ldeo.columbia.edu)

**Table 1.** Analytical approximative solutions for afterslip

	1	2	3	4	5	6
if	$q > 0$	$-1 < q < 0$	$q < -1$	$A > B$	$A > B$	$B > A$
approx	$q = \frac{V_0 t_1^*}{D_c} = \frac{A}{(B-A)k/k_c - B}$ $\dot{\theta} \ll 1/(q+1)$			$\dot{\theta} \approx \dot{\theta}_l$		$\delta \ll A\sigma/k$ and $\dot{\theta} \approx \dot{\theta}_0$
	$t_1^* > 0$	$t_1^* < 0$	$t_1^* < 0$	$V \searrow, \dot{\theta} \rightarrow$	$V \searrow, \dot{\theta} \searrow$	$V \searrow, \dot{\theta} \nearrow$
$t^*$	$t_1^* = \frac{A}{kV_0/\sigma - BV_0/D_c} = \frac{D_c A/V_0}{(B-A)k/k_c - B}$			$t_2^* = \frac{(A-B)\sigma}{kV_0} = \frac{D_c  k_c }{kV_0}$	$t_3^* = \frac{\theta_0}{\dot{\theta}_0} = \left(\frac{1}{\dot{\theta}_0} - 1\right) \frac{D_c}{V_0}$	
$\delta$	$qD_c \ln(1 + t/t_1^*)$			$\frac{D_c  k_c }{k} \ln(1 + t/t_2^*)$	$\frac{D_c}{(1-B/A)} \left(\frac{1}{\dot{\theta}_0} - 1\right) \left[ \left(1 + \frac{t}{t_3^*}\right)^{1-\frac{B}{A}} - 1 \right]$	
$V$	$\frac{V_0}{1+t/t_1^*}$			$\frac{V_0}{1+t/t_2^*}$	$\frac{V_0}{(1+t/t_3^*)^{B/A}}$	
$\theta$	$\theta_0(1 + t/t_1^*)^{-q}$			$\theta_0 + \dot{\theta}_l t$	$\theta_0 + \dot{\theta}_0 t$	
$\dot{\theta}$	$1 - \frac{\theta_0 V_0}{D_c} \left(1 + \frac{t}{t_1^*}\right)^{-q-1}$			$\dot{\theta}_l = \frac{1}{1+ k_c /k}$	$1 - \frac{\theta_0 V_0}{D_c} \left(1 + \frac{t}{t_3^*}\right)^{1-B/A}$	
$\mu$	$\mu_0 + (A + qB) \ln(V/V_0)$			$\mu_0 + (A - B) \ln(V/V_0)$		$\mu_0$

**Table 2.** Fit of afterslip data with the rate-and-state friction law. Time units is days, and displacements are expressed in m.

data	$t_{\min}$	$t_{\max}$	$t_2^{*a}$	$\delta_{\max}$	$p^b$	$A > B^c$	$B > A^c$	$B > A$ & $k < k_c^c$	$N_g/N^d$
$N_{h,S}$	1	1610	1.3	0.14	0.92	*			76/229
$N_{h,W}$	1	1610	1.0	0.16	0.88	*			45/100
$NC_{h,S}$	1	539	1.5	0.36	1.07	*	*	*	37/100
$NC_{h,W}$	1	1610	1.6	0.41	1.08	*	*	*	24/100
$SC_{h,S}$	1	1610	1.9	0.48	1.07	*	*	*	24/100
$SC_{h,W}$	1	1610	1.7	0.48	1.07	*	*	*	25/100
$SWC_{h,S}$	1	1610	1.8	0.54	1.08	*	*	*	22/100
$SWC_{h,W}$	1	1610	2	0.54	1.07	*	*	*	17/100
$FSSC_{h,BB}$	1	1233	2.2	0.46	1.13	*	*		19/285
$FSSC_{h,S}$	1	1610	2.2	0.51	1.15	*			17/200
$FSSC_{h,W}$	1	1610	5.8	0.52	1.15	*	*	*	26/200
$S_{h,S}$	1	1610	1.3	0.14	1.19	*	*	*	36/100
$S_{h,W}$	1	1610	1.3	0.14	1.18	*	*	*	44/100
$SC_{z,S}$	1	1610	0.63	0.06	1.02	*	*	*	58/100
$SC_{z,W}$	1	1610	0.74	0.05	1.04	*	*	*	69/100
$S_{z,S}$	1	1610	4.2	0.06	1.29	*	*	*	44/100
$S_{z,W}$	1	1080	3.4	0.06	1.20	*	*	*	52/100
creep <sub>h</sub>	0.0007	0.12	0.16	0.005	? <sup>e</sup>		*		27/300

<sup>a</sup> value of  $t_2^* = (A - B)\sigma/kV_0$  estimated by *Wennerberg and Sharp* [1997]

<sup>b</sup> exponent  $p = d \ln V / d \ln t$  estimated for  $5t_2^* < t < t_{\max}$ 
<sup>c</sup> a star indicates there are models in this range of model parameters that fit the data. with a residue smaller than  $\text{rms}_{\min}$ .

<sup>d</sup> Ratio of the number of models with  $\text{rms} < \text{rms}_{\min}$  and of the number of optimizations with different initial values of model parameters.

<sup>e</sup>  $p$  cannot be estimated because  $t_2^* > t_{\max}$

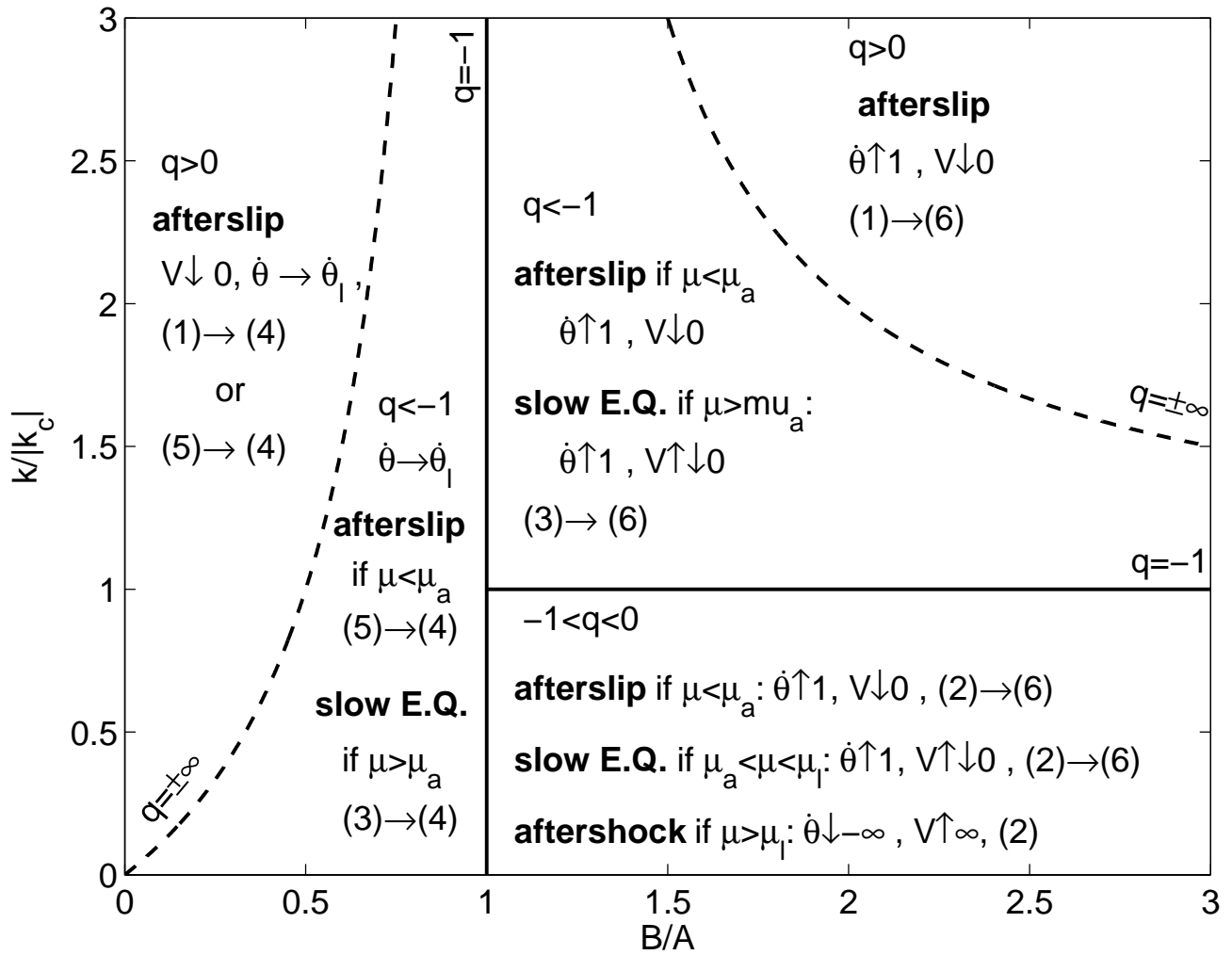
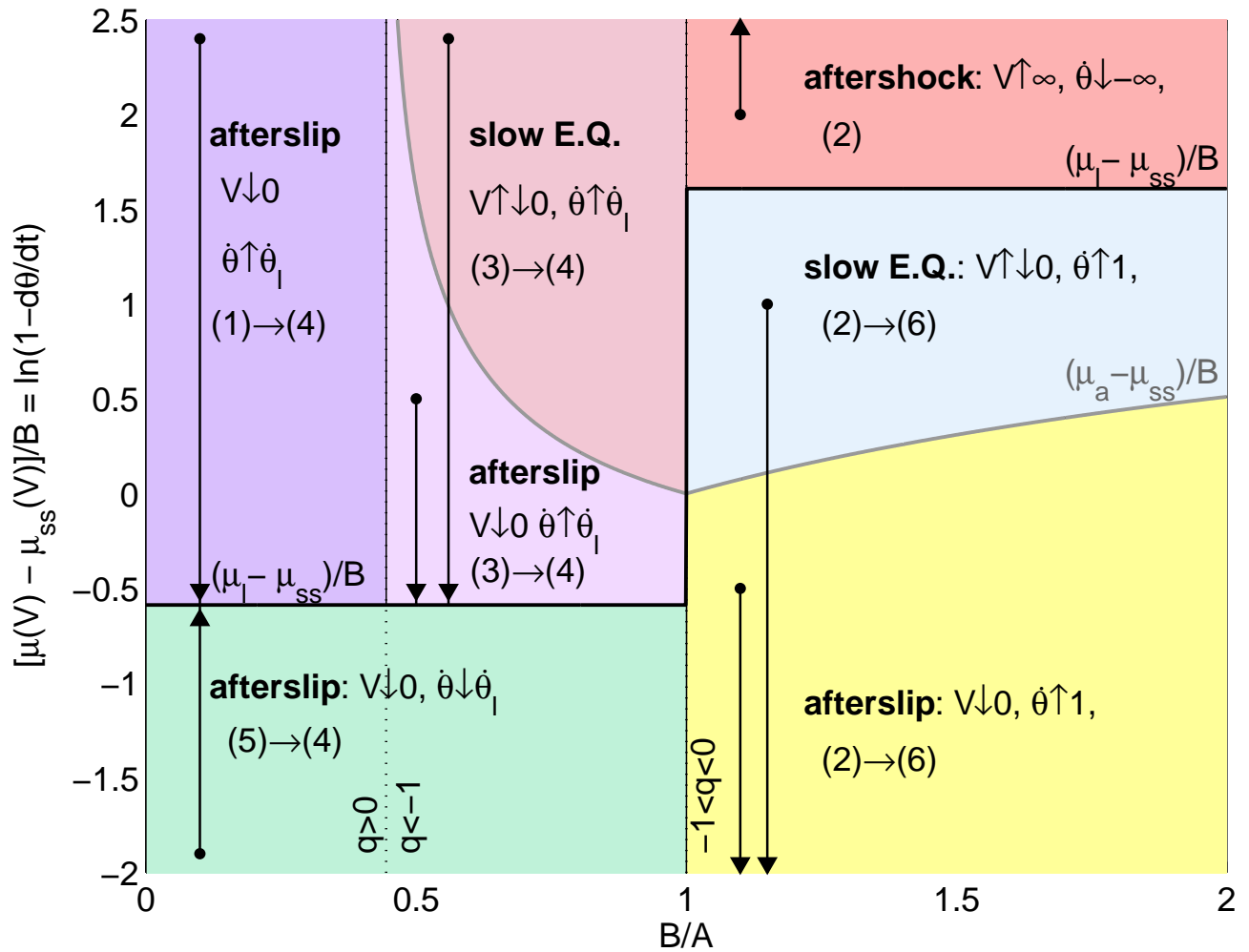


Figure 1. Value of  $q = 1/[(B/A - 1)k/k_c - B/A]$ , which controls the different postseismic behaviors (see Table 1).



**Figure 2.** Value of  $\ln(1 - \dot{\theta})$  as a function of  $B/A$  for  $k = 0.8|k_c|$ . Also shown are limits for acceleration and instability, and trajectories in this space (arrow). Numbers in brackets refer to approximate analytical solutions given in Table 1.

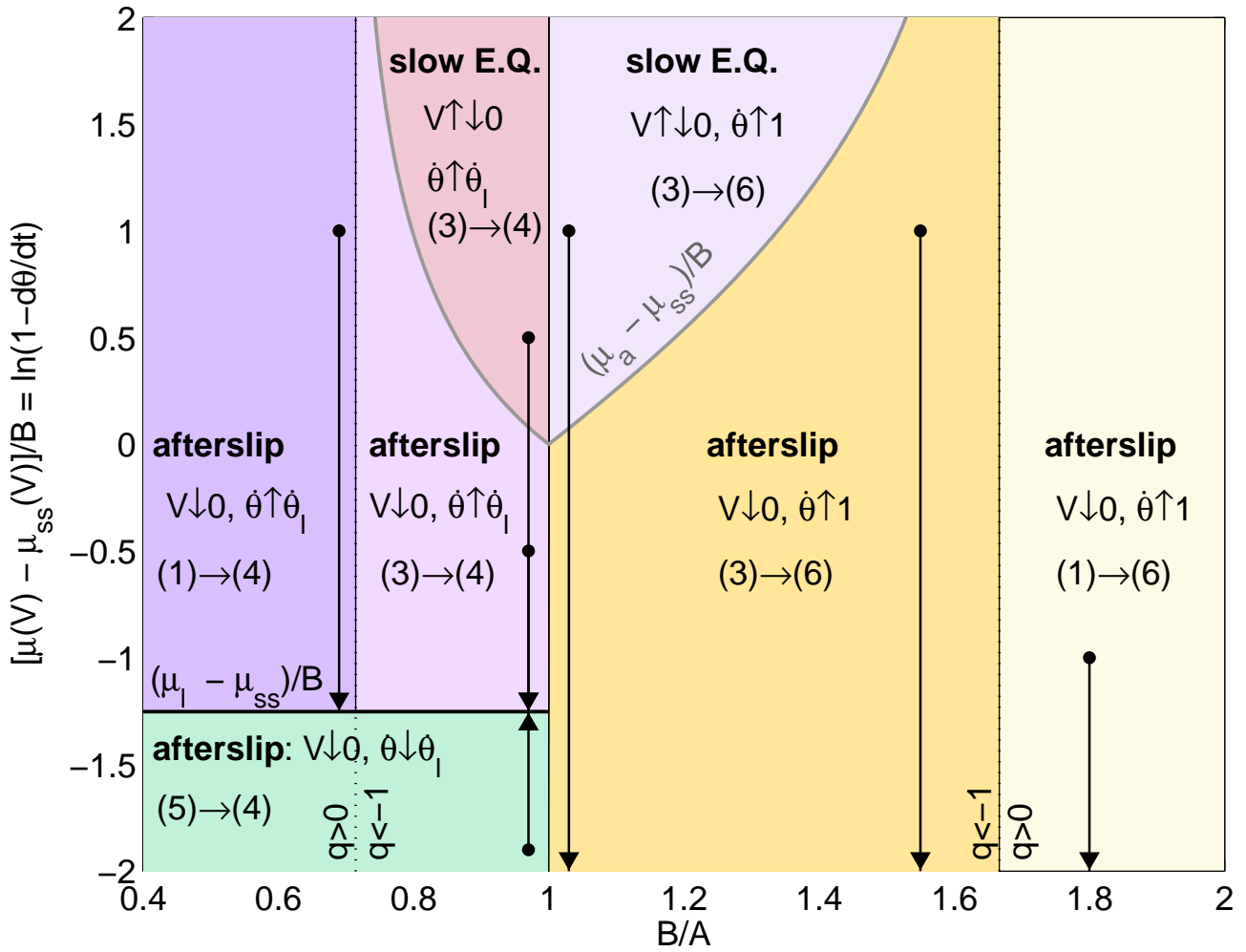
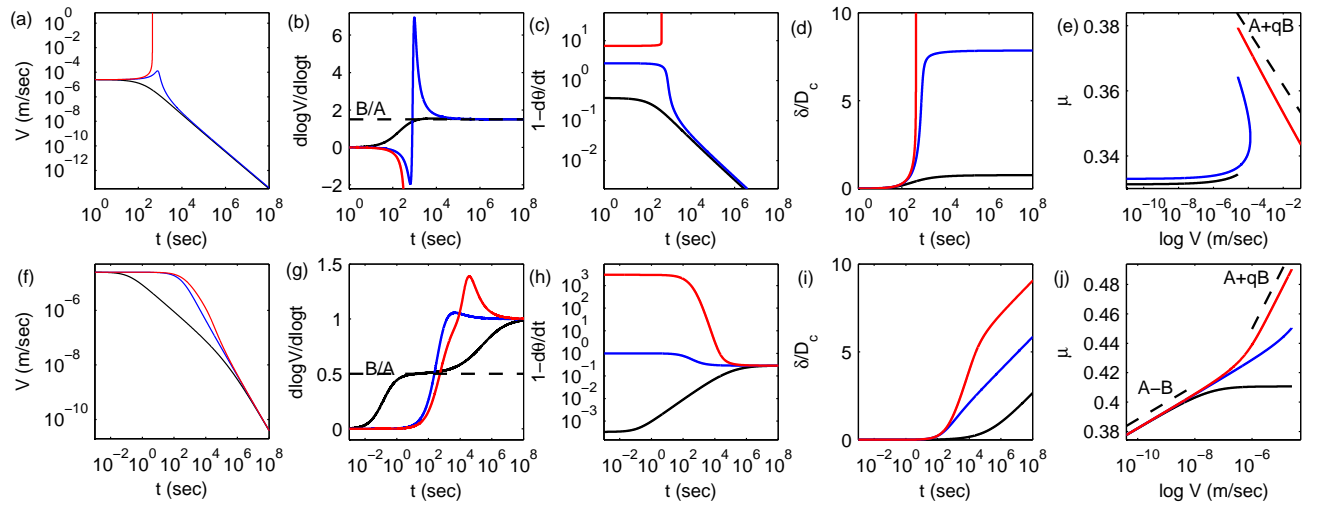
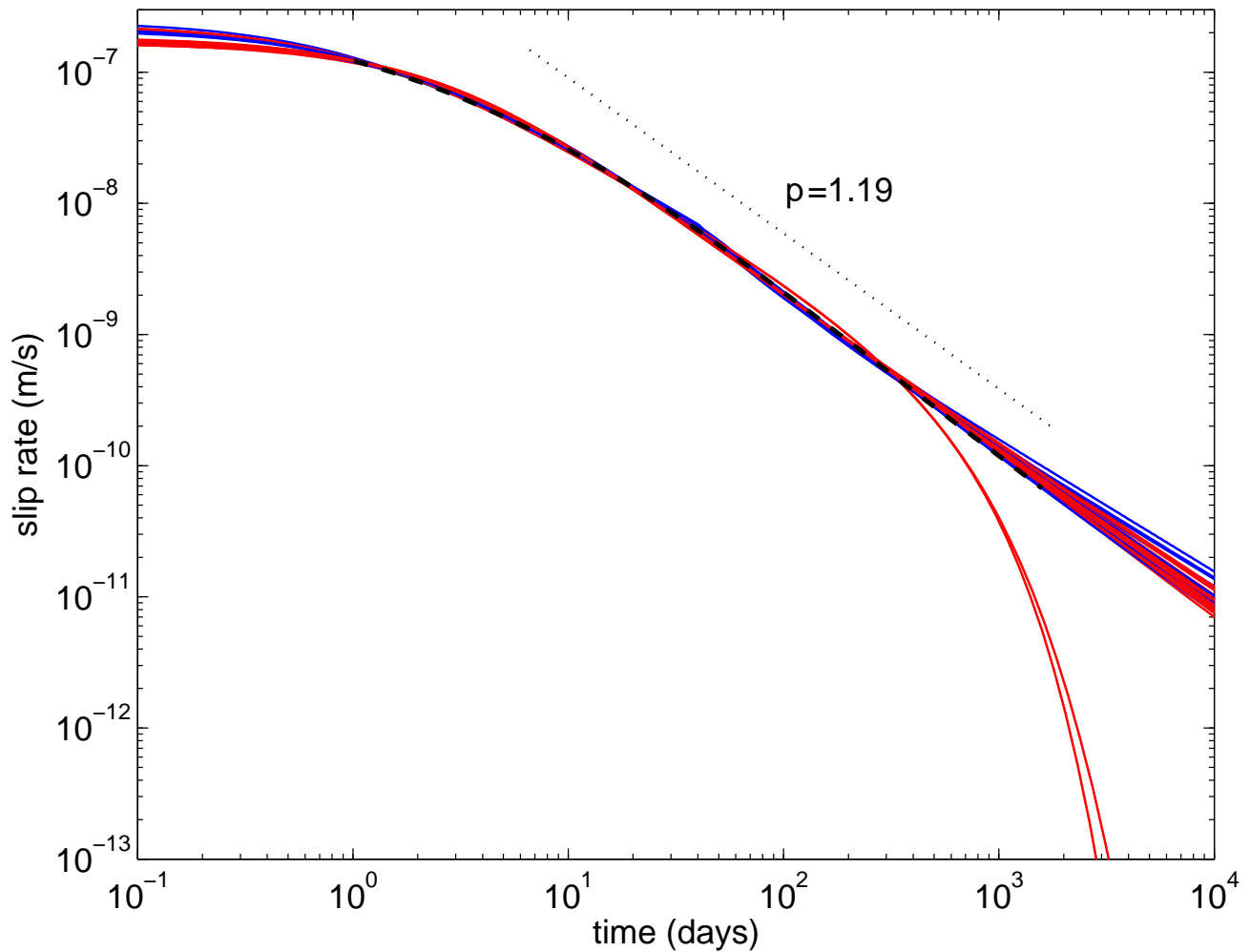


Figure 3. Same as in Figure 2 for  $k = 2.5|k_c|$ .



**Figure 4.** Temporal evolution of slip rate (a,f), slip rate exponent  $d \ln V / d \ln t$  (b,g), state rate (c,h), slip (d,i), as well as variation of friction with slip rate (e,j), for numerical simulations with  $B = 1.5A$  and  $k = 0.8k_c$  (top, a-e), and  $B = 0.5A$  and  $k = 2.5|k_c|$  (bottom, f-j). Each curve corresponds to a different value of initial friction. In (a-e), initial friction  $\mu_0$  is  $\mu_{ss}(V_0) - B$  (black curve),  $\mu_{ss}(V_0) + B$  (blue), and  $\mu_{ss}(V_0) + 2B$  (red). In (f-j),  $\mu_0$  equals  $\mu_{ss}(V_0) - 8B$  (black),  $\mu_{ss}(V_0)$  (blue), and  $\mu_{ss}(V_0) + 8B$  (red).



**Figure 5.** Observed slip rate for the  $S_{h,S}$  time series (see line 12 in Table 2) (dashed black line, for times between 1 and 1600 days), compared with all models that have a residue (for displacement) smaller than 1 mm. Models in the velocity weakening regime are shown in red, and blue for the velocity strengthening models. The dotted line is the slope measured for  $t > 6$  days.

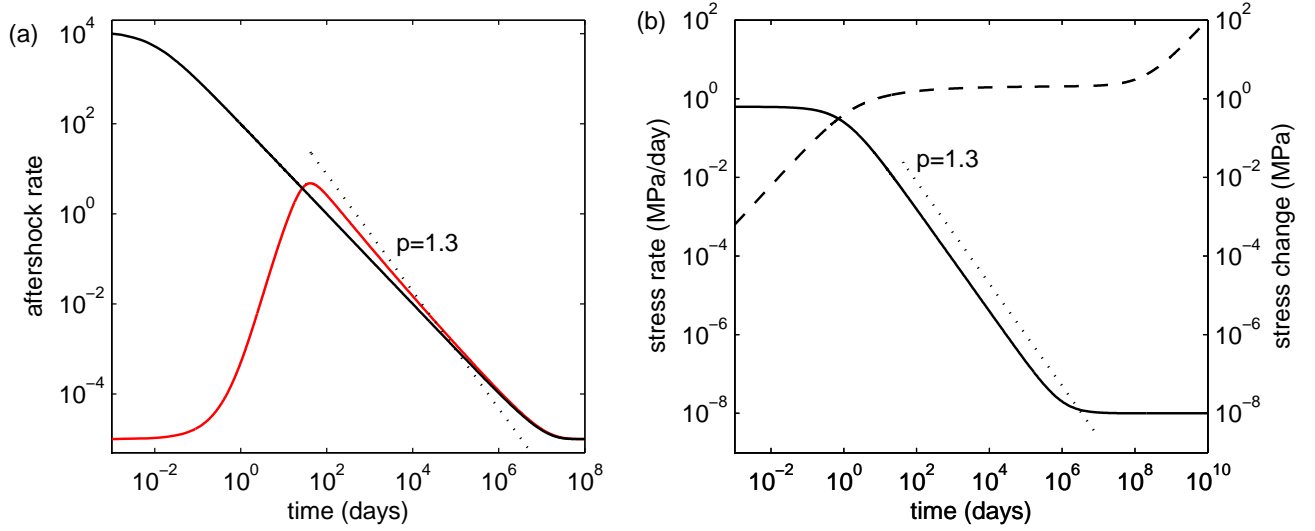


**Figure 6.** Seismicity rate (a) triggered by a continuous stress change given by  $\dot{\tau} = \dot{\tau}_0/(1 + t/t^*)^p$  (red curve) and by a simple stress step of the same amplitude  $\Delta\tau = \dot{\tau}_0 t^*/(p-1) = 2.08$  MPa (black curve). Plot (b) shows the stress rate (continuous line) and stress change (dashed line). The model parameters are  $\dot{\tau}_0 = 0.62$  MPa/day,  $t^* = 1$  day,  $\dot{\tau}_r = 10^{-8}$  MPa/day (constant stress rate) and  $A\sigma = 0.1$  MPa. This gives  $n = 6.2$ ,  $C = 10^8$ . The time  $t_{R_{\max}}$  calculated using the approximate solution (32) is 14.6 days, while the observed time when  $R$  is maximum is 42 days. The crossover time  $t_c$  given by (35) is 450 days, and marks the transition between a  $\sim 1/t^p$  decay of seismicity rate for  $t_{R_{\max}} < t < t_c$  to the long time  $\sim 1/t$  decay.

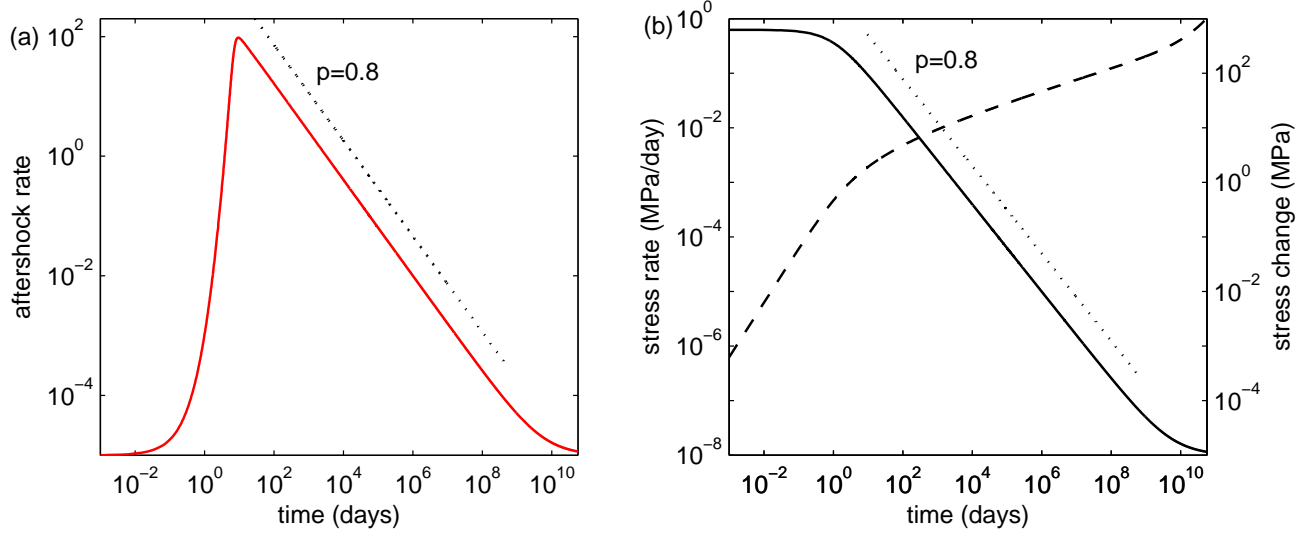


**Figure 7.** Same as in Figure 6 for  $p = 0.8$ , but with the same values of  $t^*$  and  $\dot{\tau}_0$ . The time  $t_{R_{\max}}$  calculated using the approximate solution (32) is 9.4 days, while the observed time when  $R$  is maximum is 14.6 days. The seismicity rate is proportional to the stress rate for  $t > t_{R_{\max}}$ .